

# An Aerodynamic Model-aided State Estimator for Multi-rotor UAVs

Rongzhi Wang , Danping Zou\* , Changqing Xu , Ling Pei , Peilin Liu and Wenxian Yu

**Abstract**—A robust state estimator is presented by fusing the aerodynamic model of multi-rotor UAVs with measurements from optical flow and other low-cost sensors such as IMU, magnetometer, and ultrasonic sensor. Due to the particular aerodynamics of multi-rotor UAVs, the body velocity in the rotor plane is able to be measured by the accelerometer. We therefore propose a novel state estimator by fully exploring the characteristic of aerodynamics of multi-rotor UAV. Our state estimator is fast and easy to be implemented. We have tested our estimator with different platforms in different scenes. Experimental results show that our estimator performs robustly in low light conditions where existing methods usually fail.

## I. INTRODUCTION

Multi-rotor unmanned aerial vehicles (UAV) have emerged as a popular platform for aerial photography and autonomous missions in recent years. Reliably estimating the state of the vehicle, including its orientation, position, and velocity, is crucial for a UAV to achieve a stable flight. Obtaining the position and velocity is particularly important for outer-loop flight control such as hovering and trajectory following. The most common approach to estimating position and velocity of a UAV is integrating IMU and GPS in outdoor environments. For GPS-denied environments, vision-based techniques such as visual SLAM[1][2][3], visual odometry[4][5], and optical flow[6][7] are widely used. Among all of them, optical flow has become the most popular approach because of its easy implementation and low computational cost.

Nowadays almost every professional product of multi-rotor UAV equips with an optical flow sensor. The optical flow sensor measures the horizontal velocities and with integration, the positions of the UAV. Like any other vision-based methods, optical flow is also subject to the texture richness, lighting condition of the scene. Lack of texture or sufficient light will produce noisy or false velocity estimates, making control unstable and even leading the UAV to crash. Though fusing visual measurements with inertial measurements as in many visual-inertial navigation systems [8][9] is able to increase the robustness of state estimation to some extent. A short period of bad quality of image inputs could still produce a remarkable error because only integration of inertial measurements works at that time.

In this paper, we propose a dynamic model-aided state estimator tailored for multi-rotor UAVs based on optical flow. The basic idea is to fully explore the distinctive dynamic

model of a flying multi-rotor UAV. It is known that a flying multi-rotor UAV exhibits a special aerodynamic characteristic that renders its body velocity and yaw, pitch angle observable from only IMU measurements[10][11]. Apart from optical flow, we also fuse the aerodynamic information with other sensors including gyroscope, accelerometer, magnetometer and ultrasonic sensor to produce a reliable estimate of both attitude and velocity of a flying multi-rotor UAV despite bad quality of visual inputs.

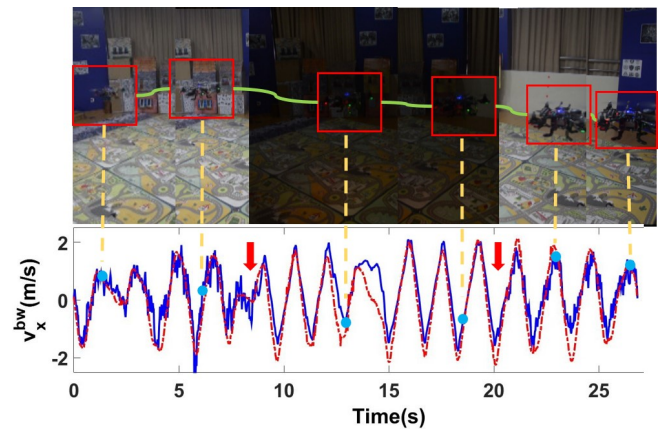


Fig. 1. Our state estimator's performance in a dark room with the lights switching on/off. The quadrotor flies in the room with lights turning on firstly. Then the light is turned off for about ten seconds and turned on later. The bottom presents velocity estimates based on our estimator (blue curve) with ground truth (red curve). The red arrow indicates the time when turning off light.

Specifically, this paper makes two main contributions. Firstly, we show how aerodynamics of multi-rotor UAVs can be employed to achieve robust and accurate results by fusing optical flow and IMU measurements in a way that is different from classic visual-inertial systems. To the best of our knowledge, this is the first time of such kind of attempt that has been verified in real-world scenes with real multi-rotor platforms. Secondly, we demonstrate that our model-aided velocity estimator is able to work in challenging scenes with low light conditions and few textures, and provides a reliable feedback source for robust flight control.

We evaluate our estimator in scenes with challenging illumination conditions using both self-built and commercial multi-rotor UAVs. Results show the efficacy and robustness of our state estimator. An example of our results is illustrated in Figure 1. The rest of this paper is organized as follows: Section II gives a brief related work on state estimation of multi-rotor UAVs. Section III presents the dynamic model of multi-rotor UAV. Section IV then describes measurement

All the authors are with Shanghai Key Laboratory of Navigation and Location Based Services, Shanghai Jiao Tong University. This work is supported by Natural Science Foundation of China (Grant No. 61402283), Shanghai Science and Technology Committee (15511105100, 17DZ1100803), and National Science and Technology Major Project (GFZX0301010708).

\*Corresponding author: Danping Zou, Email: dpzou@sjtu.edu.cn

model for each sensor used in our state estimator, including accelerometer, gyroscope and optical flow. The detail of our estimator is given in Section V. Flight experiments are presented in Section VI. The conclusion is drawn in Section VII

## II. RELATED WORK

A robust state estimator for a multi-rotor UAV that is capable of working in GPS-denied environments has drawn numerous research for many years. Because video cameras are ubiquitous, cheap, capturing rich information of the environment, vision-based state estimator has been increasingly popular for applications of aerial vehicles. Vision-based techniques like visual SLAM [3][12], visual odometry [5] or their extensions [13] that integrated with IMU measurements become a promising solution to robust navigation within GPS-denied environments.

Typical visual SLAM/odometry systems require a complicate pipeline involving landmark extraction, recursive pose estimation and map update, as well as a time-consuming back-end optimization. The high computational cost prohibits SLAM-based methods from being applied to low-end platforms. Optical flow [14] is however a good alternative with low computational complexity. Though optical flow only measures the pixel displacement between successive video frames, integrated with an altitude sensor like ultrasonic or Time-of-Flight (ToF) range sensors, it works well as a 3D speed or position sensor. It has been shown that with some special treatments, optical flow can run on low-end embedded systems at the rate of 200 fps[15], make it suitable for all sorts of multi-rotor UAVs.

Though vision-based methods has achieved great success in state estimation of multi-rotor UAVs. Bad quality of visual inputs, such as lack of texture, low lighting condition and saturated exposure, will cause fatal failure for vision-based algorithms. A straightforward solution is fusing measurements from other sensors [16][17] to improve the robustness. While lots of fusion algorithms have been proposed, few of them take into account the aerodynamics of multi-rotor UAVs.

In fact, multi-rotor UAV's special dynamic characteristic makes its body velocity observable from only IMU measurements [18]. Specifically, the body velocity of a multi-rotor UAV projected in the propeller plane is approximately proportional to the accelerator measurements. Based on this principle, a number of observers have been proposed to estimate translation velocity and roll, pitch angles from only inertial sensors [19][20]. Others also seek to integrate sensors other than inertial sensors such as ultra-wide band ranging radios [21] and barometer [22] to get more accurate results. Novel visual-inertial systems built on existing visual SLAM systems incorporating dynamic model of multi-rotor UAVs have been proposed [9][23]. As we have stated, SLAM systems usually incur heavy computation, which requires high-performance hardware.

A recent approach [8] takes a step further to fuse the dynamic model with the epipolar geometry between successive images. This approach achieves remarkable efficiency with

nearly 100Hz visual update rate on Odroid U3 development board. But the filter may diverge if the two images chosen for EKF update have insufficient disparity, particularly when the UAV is hovering or rotating. Our estimator is however built on current optical flow technique that has been proved as efficient and effective. By incorporating the dynamic model of multi-rotor UAV, our estimator is able to work in challenging scenes where existing optical flow estimators usually fail, without bringing in extra computational costs.

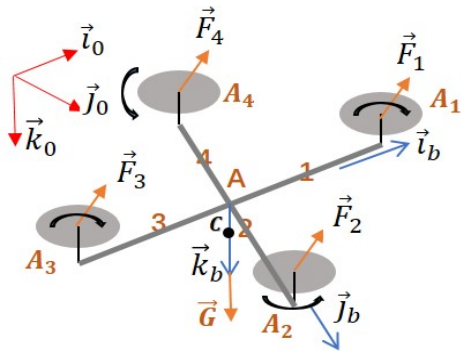


Fig. 2. Illustration of notations on a quadrotor.

## III. AERODYNAMICS OF MULTI-ROTOR UAVS

In this section, we briefly review the aerodynamic model of multi-rotor UAVs. For more details, we refer interested readers to the work [18]. Though the aerodynamic model holds for all multi-rotor UAVs, here we take quadrotor as an example to derive the dynamic model for simplicity. Quadrotor has four propellers fixed in a rigid frame symmetrically, with one pair of propellers rotating counter-clock-wise and the other pair clock-wise as shown in Fig. 2. Each propeller has a geometric center  $A_i$  and a rotor plane perpendicular to the normal unit vector  $\vec{k}_b$  of rigid frame of quadrotor, of which the geometry center is  $A$ .  $\omega_i$  is the spinning speed of  $i$ -th propeller, with  $\varepsilon_i = 1$  for counter-clock-wise and  $\varepsilon_i = -1$  vice versa. The gravity center of the quadrotor is located at  $C$ . Following the momentum theory and blade element theory in [24], the aerodynamic force generated by four propellers is written as

$$\sum_{i=1}^4 \vec{F}_i \approx -\alpha \left( \sum_{i=1}^4 \omega_i^2 \right) \vec{k}_b - \lambda \left( \sum_{i=1}^4 \omega_i \right) \vec{V}_C^\perp. \quad (1)$$

Where  $\alpha, \lambda$  are constant parameters depend on the material, structure of propellers and air density.  $\vec{V}_C$  is the translation velocity of quadrotor gravity center and Notation  $(\cdot)^\perp$  denotes the projection of a given vector on the rotor plane. The approximation in (1) is based on the assumption of low flight velocity and approximately the same spinning speed of four propellers [18]. The first term of (1) is the total thrust generated by all propellers, causing the upward motion acceleration. The second term is so called  $H$ -force drag that can be directly measured by an accelerometer as we'll discuss in Section IV-B.

According to Newton's law, the total force applied on the gravity center of quadrotor is given by

$$\vec{F}_C = m\dot{\vec{V}}_C = m\vec{G} - \alpha \left( \sum_{i=1}^4 \omega_i^2 \right) \vec{k}_b - \lambda \left( \sum_{i=1}^4 \omega_i \right) \vec{V}_C^\perp. \quad (2)$$

We use a superscript  $w$  to denote the world frame, and  $b$  the body-fixed frame. Denoting the rotation matrix from body-fixed frame to world frame by  $R_b^w$ , we have  $\vec{V}_C = R_b^w \vec{V}_C^b$ . Taking derivative w.r.t time on both side, this yields

$$\dot{\vec{V}}_C = R_b^w \vec{\omega} \times \vec{V}_C^b + R_b^w \dot{\vec{V}}_C^b \quad (3)$$

where  $\vec{\omega}$  is angular velocity of the UAV, which can be measured by a gyroscope. Substituting Equation (3) to (2) and denoting the velocity of quadrotor in body frame by  $\vec{V}_C^b = (v_x, v_y, v_z)^T$ , we obtain

$$\dot{\vec{V}}_C^b = \vec{G}^b + \frac{\vec{T}_{thrust}^b}{m} + \frac{\vec{T}_{drag}^b}{m} - \vec{\omega}^b \times \vec{V}_C^b. \quad (4)$$

Here  $\vec{G}^b$  is the gravity vector expressed in body-fixed frame written as

$$\vec{G}^b = -\sin\theta \vec{i}_b + G \cos\theta \sin\phi \vec{j}_b + G \cos\theta \cos\phi \vec{k}_b. \quad (5)$$

Here  $\vec{i}_b, \vec{j}_b$ , and  $\vec{k}_b$  are three orthogonal axes as shown in Fig.2 expressed in the world frame. Equation (4)-(5) yield the dynamical model of a flying multi-rotor UAV:

$$\begin{aligned} \dot{\vec{V}}_C^b = & (-G \sin\theta - \mu \cdot v_x^b - (\omega_y^b v_z^b - \omega_z^b v_y^b)) \vec{i}_b \\ & + (G \cos\theta \sin\phi - \mu \cdot v_y^b - (\omega_z^b v_x^b - \omega_x^b v_z^b)) \vec{j}_b \\ & + (G \cos\theta \cos\phi - a_z - (\omega_x^b v_y^b - \omega_y^b v_x^b)) \vec{k}_b \end{aligned} \quad (6)$$

where  $\mu = \frac{\lambda(\sum_{i=1}^4 \omega_i^2)}{m}$  and  $a_z = \frac{\alpha(\sum_{i=1}^4 \omega_i)}{m}$ . The first variable  $\mu$  is the drag coefficient that relates the body velocity in rotor plane to the accelerometer measurements as we'll show in the later section. The second variable  $a_z$  is the upward acceleration that is measured by an accelerometer. Our estimator adopts (6) as the prediction model in the Extended Kalman Filter.

#### IV. SENSORS

The proposed estimator fuses measurements from different sensors including gyroscope, accelerometer and optical flow in an Extended Kalman filter (EKF). This section will discuss each sensor model and reveal their relation to state of the multi-rotor UAV.

##### A. Rate Gyroscope

The angular velocity of rigid frame in body coordinates is measured by on-board gyroscope. For simplicity, we assume the triad of gyroscope is perfectly aligned with the three axes of the body of UAV. The gyroscope is modeled as

$$\tilde{\omega}_i = \omega_i + \beta_{g_i} + \delta_{g_i} \quad (7)$$

$$\dot{\beta}_{g_i} = -\frac{1}{\tau_{g_i}} \beta_{g_i} + \delta_{\beta_{g_i}} \quad (8)$$

where  $i = \{x, y, z\}$ ,  $\tilde{\omega}_i$  is the measured angular velocity and  $\omega_i$  is the true value and  $\beta_{g_i}$  represents the sensor bias. Equation (8) describes the bias error model and  $\tau_{g_i}$  parameterizes the changing speed of bias. The last terms of both equations,  $\delta_{g_i}, \delta_{\beta_{g_i}}$  are zero-mean white Gaussian noises. With Euler angle representation, the attitude or orientation of the UAV can be estimated from gyroscope measurements by solving the differential equation

$$\begin{bmatrix} \dot{\phi} \\ \dot{\theta} \\ \dot{\psi} \end{bmatrix} = \begin{bmatrix} 1 & \tan\theta \sin\phi & \tan\theta \cos\phi \\ 0 & \cos\phi & -\sin\phi \\ 0 & \sin\phi/\cos\theta & \cos\phi/\cos\theta \end{bmatrix} \begin{bmatrix} \omega_x \\ \omega_y \\ \omega_z \end{bmatrix}. \quad (9)$$

##### B. Accelerometer

Accelerometer measures non-gravitational force in inertial space [19]. An accelerometer fixed on a UAV platform measures aerodynamic force acted upon the UAV, expressed in body-fixed coordinate system, which yields

$$\vec{a} = R_b^w \dot{\vec{V}}_C - \vec{G}^b + \vec{\beta}_a + \vec{\delta}_a, \quad (10)$$

where  $\vec{a}$  is the measurements of accelerometer,  $\vec{\beta}_a$  is bias and  $\vec{\delta}_a$  is Gaussian white noise. Putting (2), (3), and (10) together, we get the relationship between the body velocity of the UAV and accelerometer measurements as

$$\begin{aligned} \tilde{a}_x &= -\mu \cdot v_x^b + \beta_{a_x} + \delta_{a_x} \\ \tilde{a}_y &= -\mu \cdot v_y^b + \beta_{a_y} + \delta_{a_y} \\ \tilde{a}_z &= -a_z + \beta_{a_z} + \delta_{a_z}, \end{aligned} \quad (11)$$

where  $\mu$  is the drag coefficient that is related to the rotor speed as described previously. Assuming the rotor speed is kept nearly constant during flight, we can see that the body velocity in the rotor plane is approximately proportional to the accelerometer measurements in  $x$  and  $y$  axes. In other words, with the special aerodynamics of multi-rotor UAV, the body velocity can be observed directly from only accelerometer measurements, which provides valuable information to design a robust velocity estimator.

##### C. Magnetometer

An magnetometer can be used to estimate the heading of the UAV by sensing the magnetic field of the earth. Let  $\vec{m}^b$  be the magnetic direction measured in the body frame, and  $\vec{m}^w$  is the direction expressed in world frame. After transforming the  $\vec{m}^b$  to the world frame, we obtain the  $y$  component of  $\vec{m}^b$ :

$$\begin{aligned} m_y^w = & \sin\psi \cdot (m_x^b \cos\theta + m_y^b \sin\theta \sin\phi + m_z^b \sin\theta \cos\phi) \\ & - \cos\psi \cdot (-m_y^b \cos\phi + m_z^b \sin\phi), \end{aligned} \quad (12)$$

where  $\psi$  represents the yaw angle of the UAV. We align the  $x$  axis of world frame with magnetic direction, hence we have  $m_y^w = 0$ , which yields

$$\tan\psi = \frac{-m_y^b \cos\phi + m_z^b \sin\phi}{m_x^b \cos\theta + m_y^b \sin\theta \sin\phi + m_z^b \sin\theta \cos\phi}. \quad (13)$$

#### D. Optical flow

Optical flow is a motion field on the image plane which is the projection of displacement of 3D points during a short time period. The displacement of a image point, denoted by  $\Delta p_x$  and  $\Delta p_y$ , is related to the velocity of the UAV by the following equation [15].

$$\begin{aligned}\frac{\Delta p_x}{\Delta t} &= \frac{v_z^b p_x - v_x^b f}{h} - \omega_y^b f + \omega_z^b p_y + \frac{\omega_x^b p_x p_y - \omega_y^b p_x^2}{f} \\ \frac{\Delta p_y}{\Delta t} &= \frac{v_z^b p_y - v_y^b f}{h} + \omega_x^b f - \omega_z^b p_x + \frac{\omega_x^b p_y^2 - \omega_y^b p_x p_y}{f},\end{aligned}\quad (14)$$

where  $h$  is the distance between the 3D point and the camera center and  $f$  is the focus length that can be calibrated in advance. Assuming those points are mostly on the ground, by taking the average displace of all image points and ignoring the second order terms, it yields

$$\begin{aligned}v_x^b &= -\frac{\Delta \tilde{p}_x}{\Delta t} \frac{h}{f} - \omega_y^b h \\ v_y^b &= -\frac{\Delta \tilde{p}_y}{\Delta t} \frac{h}{f} + \omega_x^b h.\end{aligned}\quad (15)$$

Here,  $h$  represents the distance between the camera center and the ground. Though without dealing with each image point individually, it has been shown that this approximation still produces high accurate velocity estimation [25]. Another advantage is that using only one equation (15) for all points limits the dimension of measurement model in the filter and allows fast computation. The distance to the ground  $h$  is measured by an ultrasonic sensor or a time-of-flight (ToF) sensor accompany with the camera, which is located at the bottom of a UAV and facing downward.

#### V. ESTIMATOR DESIGN

We use an Extended Kalman Filter to fuse the measurements from gyroscope, accelerometer and optical flow, as well as ultrasonic sensor. The state of filter is defined as

$$\mathbf{x} = [\phi \ \theta \ \psi \ \beta_{g_x} \ \beta_{g_y} \ \beta_{g_z} \ v_x^b \ v_y^b \ v_z^b \ h \ \mu_x \ \mu_y]^T, \quad (16)$$

representing attitude, gyroscope bias, body velocity, the distance from ground, and drag coefficients respectively. Notice that we include two drag coefficients  $\mu_x, \mu_y$  in the state. The reason is that we find in practice that the drag coefficient is different for  $\vec{i}_b$  and  $\vec{j}_b$  axes in the rotor plane. It is probably caused by imperfect symmetry of the UAV platform. We therefore use two drag coefficients in our estimator, corresponding to the two directions on the rotor plane. Including the drag coefficients in the filter aims to account for their noisy value due to changing spinning speed of rotors in flight. Including the distance to the ground (or the height) in the state could also lead to better optical measurements (15). From above definition, we can see that our estimator calculates both attitude and velocity, and fulfills the requirements from both inner loop and outer loop control of multi-rotor UAVs.

#### A. Prediction Model

A typical prediction model of an Extended Kalman Filter can be written as  $\dot{\mathbf{x}} = \mathbf{f}(\mathbf{x}, \mathbf{n})$ , where  $\mathbf{n}$  is the noise vector  $\mathbf{n} \sim \mathcal{N}(\mathbf{0}, \Sigma)$ . We can derive prediction models for attitude, gyroscope bias and velocity from (9)(8)(6) respectively. The height of camera center  $h$  can be predicted by the following equation

$$\dot{h} = R_b^w \vec{V}_C^b \cdot \vec{e}_3 \quad (17)$$

where  $\vec{e}_3 = (0, 0, 1)^T$ . And the two drag coefficients are simply treated as random walk variables, namely  $\dot{\mu}_x = \delta \mu_x$  and  $\dot{\mu}_y = \delta \mu_y$ . Putting all predictions together, we get the full prediction model  $\mathbf{f}(\mathbf{x}, \mathbf{n})$  as

$$\begin{cases} \dot{\phi} = \hat{\omega}_x^b + \hat{\omega}_y^b \tan \theta \sin \phi + \hat{\omega}_z^b \tan \theta \cos \phi \\ \dot{\theta} = \hat{\omega}_y^b \cos \phi - \hat{\omega}_z^b \sin \phi \\ \dot{\psi} = \hat{\omega}_y^b \sin \phi / \cos \theta + \hat{\omega}_z^b \cos \phi / \cos \theta \\ \dot{\beta}_{g_x}^b = -\frac{1}{\tau_{g_x^b}} \beta_{g_x}^b + \delta \beta_{g_x} \\ \dot{\beta}_{g_y}^b = -\frac{1}{\tau_{g_y^b}} \beta_{g_y}^b + \delta \beta_{g_y} \\ \dot{\beta}_{g_z}^b = -\frac{1}{\tau_{g_z^b}} \beta_{g_z}^b + \delta \beta_{g_z} \\ \dot{v}_x^b = -g \sin \theta + \mu_x v_x^b - (\hat{\omega}_y^b v_z^b - \hat{\omega}_z^b v_y^b) \\ \dot{v}_y^b = g \cos \theta \sin \phi + \mu_y v_y^b - (\hat{\omega}_z^b v_x^b - \hat{\omega}_x^b v_z^b) \\ \dot{v}_z^b = g \cos \theta \cos \phi + a_z - (\hat{\omega}_x^b v_y^b - \hat{\omega}_y^b v_x^b) \\ \dot{h} = -\sin \theta v_x^b + \cos \theta \sin \phi v_y^b + \cos \theta \cos \phi v_z^b \\ \dot{\mu}_x = \delta \mu_x \\ \dot{\mu}_y = \delta \mu_y, \end{cases} \quad (18)$$

where we let  $\hat{\omega}_i = \tilde{\omega}_i - \beta_{g_i} - \delta_{g_i}$  ( $i = x, y, z$ ) for brevity. We can see that the noise vector is  $\mathbf{n} = (\delta_{g_x}, \delta_{g_y}, \delta_{g_z}, \delta \beta_{g_x}, \delta \beta_{g_y}, \delta \beta_{g_z}, \delta \mu_x, \delta \mu_y)^T$ . The discrete-time prediction of the state  $\mathbf{x}_t$  is computed by Euler method, namely  $\mathbf{x}_t = \mathbf{x}_{t-1} + \mathbf{f}(\mathbf{x}_{t-1}, \mathbf{0}) \Delta t$ . Of course high-order methods like Runge-Kutta method can be adopted to achieve better accuracy. The covariance is propagated by  $\mathbf{P}_t = \mathbf{F}_x \mathbf{P}_{t-1} \mathbf{F}_x^T + \mathbf{G}_n \Sigma \mathbf{G}_n^T$ , where  $\mathbf{F}_x = \partial \mathbf{f} / \partial \mathbf{x} \Delta t$  and  $\mathbf{G}_n = \partial \mathbf{f} / \partial \mathbf{n} \Delta t$ . The covariance  $\Sigma$  is a diagonal matrix which can be estimated beforehand.

#### B. Measurement Model

Equation (11)(15)(13) provide measurements of velocity and yaw angle of the multi-rotor UAV. The ultrasonic sensor provides additional measurements of the distance to the ground. Put them together, we obtain the full measurement model as

$$\begin{cases} \tilde{a}_x = \mu_x \cdot v_x^b + \delta_{a_x^b} \\ \tilde{a}_y = \mu_y \cdot v_y^b + \delta_{a_y^b} \\ \tilde{v}_x^b = v_x^b + \delta_{v_x^b} \\ \tilde{v}_y^b = v_y^b + \delta_{v_y^b} \\ \tilde{\psi} = \psi + \delta_{\psi} \\ \tilde{h} = h + \delta_h \end{cases} \quad (19)$$

where  $\tilde{v}_x^b$  and  $\tilde{v}_y^b$  are estimated optical flow (15) and  $\delta_{v_x^b} \sim \mathcal{N}(0, \sigma^2)$ ,  $\delta_{v_y^b} \sim \mathcal{N}(0, \sigma^2)$  are the estimation noises. The measurement variance  $\sigma^2$  is adaptive to the quality of optical

flow as in the implementation of [15]. It computes optical flow for 25 sub image blocks. Those blocks with low variance of intensities and large sum of absolute difference (SAD) with corresponding blocks in the next frame are marked as 'bad' blocks. The quality of optical flow is measured by the percentage of good blocks normalized by multiplying a constant 255, namely

$$Q = 255 \cdot (1 - N_{bad}/25) \quad (20)$$

In our implementation, the flow measurement variance  $\sigma^2$  is set empirically as

$$\sigma^2 = \sigma_{norm}^2 \cdot \exp(Q/Q_{norm} - 1) \quad (21)$$

where  $\sigma_{norm}^2$  and  $Q_{norm}$  are flow covariance and quality estimated in normal lighting conditions.

The yaw angle  $\psi$  is estimated from (13) and the height  $\hat{h}$  comes from the ultrasonic sensor. The variances of noises  $\delta_\psi$  and  $\delta_h$  can be acquired by calibration (comparing the measured values with the ground-truth values, for example from the motion capture system).

## VI. EXPERIMENT

We test the proposed estimator using both home-made and commercial platforms. Our self-built platform is shown in the left in Fig. 3, which uses an open-source Pixhawk flight management unit [26], an invensense MPU9250 containing a 3-axis accelerometer, a 3-axis gyroscope and a 3-axis magnetometer, and an optical flow sensor PX4FLOW[15] that includes a machine vision CMOS image sensor and an ultrasonic sensor. The proposed estimator runs on the on-board computer Odroid U3. The commercial platform is the Parrot's ARDrone 2.0. It equips with an IMU as well as a camera and a ultrasonic sensor at the bottom. We acquire the sensor data through the Wifi connection to the drone and run our estimator on a laptop with an i5-4210U CPU (1.7GHz, 4 core) in real time.

We conduct experiments in a small room and a large hall. The room is equipped with a motion capture system Vicon, which provides highly accurate position and orientation measurements of the flying UAV at 200 Hz. In the large hall, we put some recognizable tags on the ground, and manually control the drone to fly over them. The positions of those tags are treated as ground truth. Meanwhile, we provide a demo video which gives a clear summary of our experiments accompanied with this paper.

### A. Drag coefficients initialization

Before running our estimator, we need to obtain an initial value of the aerodynamic coefficients  $\mu_x$  and  $\mu_y$ . We collect flight data from our quadrotor and compare them with the ground truth from Vicon. The drag coefficients are estimated by linear fitting,

$$\begin{aligned} \tilde{\mu}_x &= \min_{\mu_x} (\tilde{a}_x - \mu_x v_x^b)^2 \\ \tilde{\mu}_y &= \min_{\mu_y} (\tilde{a}_y - \mu_y v_y^b)^2 \end{aligned} \quad (22)$$

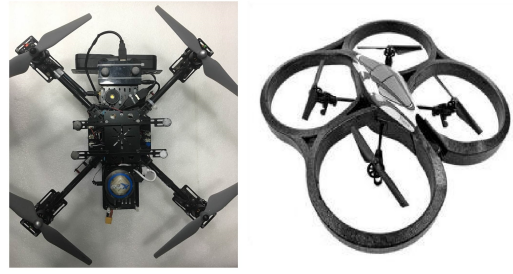


Fig. 3. Platforms used in experiments. The left is the platform developed by our team. The right is ARDrone2.0

where the  $v_x^b$  and  $v_y^b$  are from vicon data. Fig. 4 shows the line fitting results for our UAV platform. In our experiments, the drag coefficients are initialized by  $\mu_x = -0.2748$ ,  $\mu_y = -0.2498$  for our platforms and  $\mu_x = -0.6751$ ,  $\mu_y = -0.6482$  for ARDrone.

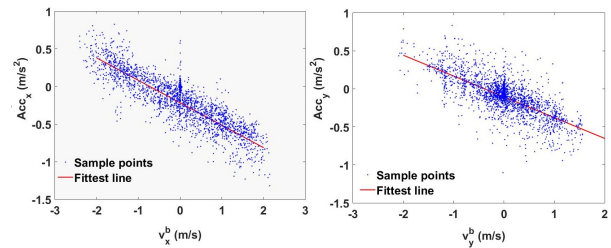


Fig. 4. Drag coefficients initialization by line fitting. Left: line fitting of  $\mu_x$ . Right: line fitting of  $\mu_y$ .

### B. Manual flight with controlled lighting condition

In this experiment, we want to evaluate the performance of our estimator in various lighting conditions. The experiment is conducted in a Vicon room at night. We test our estimator in a flight where the lights of room are firstly turned on, and suddenly turned off. The results are shown in Fig. 5. When the lights are turned on, the scene is bright enough to allow optical flow to work properly. It can be seen before turning off the lights (0 ~ 35s), the velocity estimation error of optical flow is close to that of the proposed estimator. Incorporation of aerodynamic model still improves the estimation accuracy - the average estimation error of optical flow is  $0.355m/s$  (with standard deviation of  $0.322m/s$ ) while the average error of the proposed estimator is  $0.275m/s$  (with standard deviation of  $0.280$ ). After turning of the light, the performance of optical flow degrades significantly to  $0.893m/s$  (with standard variance of  $1.426$ ) because the scene becomes complete dark. From the plot in Fig.5(b), we can see in fact that velocity estimation of optical flow becomes noises. In comparison, the proposed estimator still produces estimates that are close to the ground truth as shown in Fig. 5(a), with a slightly larger error of  $0.349m/s$  (with standard variance of  $0.142$ ). We also evaluate the attitude estimation performance of our estimator. The results are shown in Fig. 6. The observable errors in yaw estimation

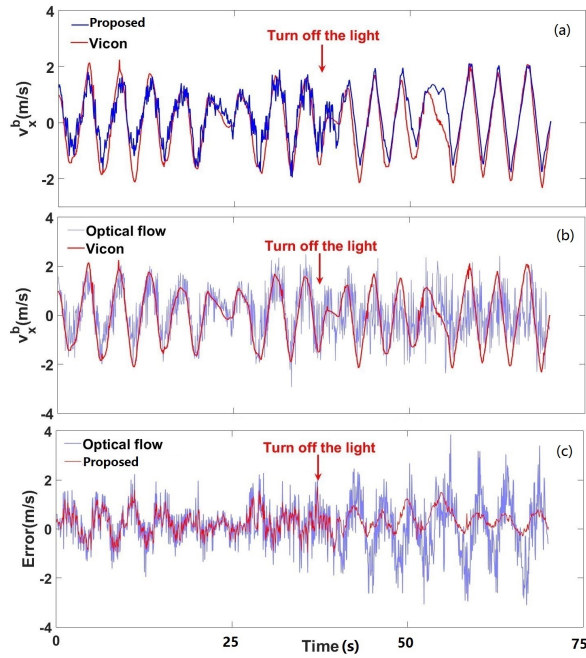


Fig. 5. Results of velocity estimation in changing lighting condition. (a) Result of the proposed estimator (blue) and the ground truth (red); (b) Result of optical flow (blue) and the ground truth (red); (c) Error comparison between optical flow and the proposed estimator.

are most likely explained by magnetometer’s sensitivity to magnetic field in environment.

### C. Autonomous flight in complete darkness

In this experiment, quadrotor flies along a horizontal  $2.4m \times 2.4m$  ‘L’ path in the dark room. The ‘L’ path is shown as the purple line in Fig. 7. We here use ARDrone to follow the ‘L’ path automatically. The actual flight trajectory using the proposed estimator is shown in Fig. 7. The results show that autonomous flight can be achieved in the extreme condition using our estimator, though error exists in path following. We attempt to use the velocity estimation from ARDrone for autonomous flight but always fail. For comparison, we also show the velocity estimation from ARDrone side-by-side in Fig. 7. The velocity estimation in three directions are also plotted in Fig. 8.

### D. Manual flight in a large dark hall

In this experiment, the quadrotor is controlled manually to fly along a  $8.12m \times 6.5m$  rectangle in a large hall in the low light condition. Without the help of motion capturing system, we put four tags on each corner of the rectangle path as shown in Fig. 9 which can be used to decide when the quadrotor is flying over each tag using downward camera. The duration of flight is about  $35s$  each round, where the average velocity is about  $1.7m/s$ . We compare our estimator with the one provided by ARDrone itself. The results are shown in Fig. 10. The total traveling distance is about  $26m$ . We can see that ARDrone produces poor velocity estimation which leads to a  $4.13m$  drifting error and only  $16.00m$

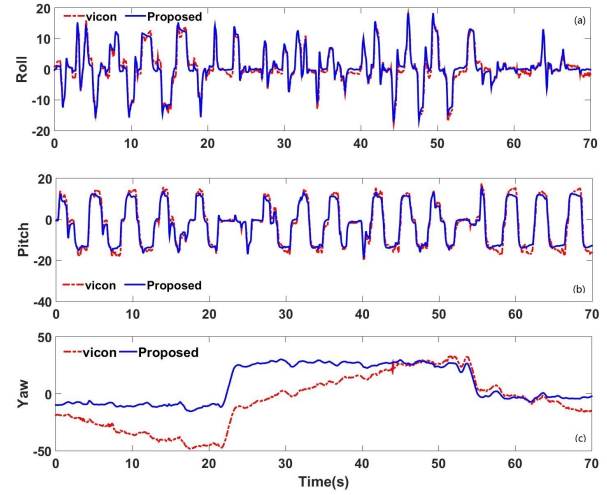


Fig. 6. Attitude estimation results of the proposed estimator. Top: roll angle estimation with mean error  $0.235^\circ$  and standard deviation  $1.359^\circ$ . Middle: pitch angle estimation with mean error  $0.172^\circ$  and standard deviation  $2.024^\circ$ . Bottom: yaw angle estimation with mean error  $14.79^\circ$  and standard deviation  $13.70^\circ$ .

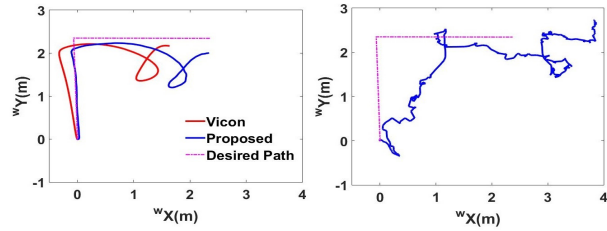


Fig. 7. Autonomous flight along a ‘L’ path in complete darkness. The left shows actual path measured by vicon (red) and the estimation produced by our estimator (in blue). For comparison, the native velocity estimation from ARDrone is shown in the right.

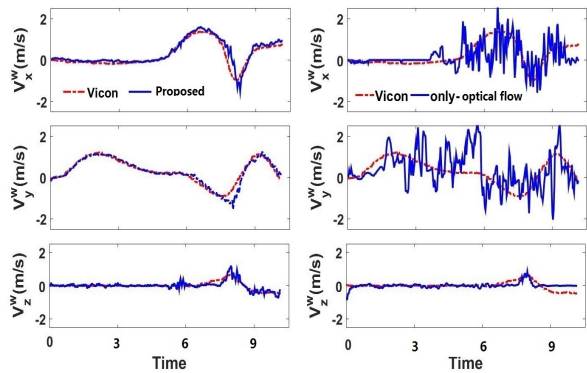


Fig. 8. Velocity estimates and ground truth for ‘L’ autonomous flight in dark room. Left: world-fixed velocity estimates using our estimator; Right: velocity estimates from ARDrone. From top to bottom: velocity in  $X, Y, Z$  directions.



Fig. 9. Four tags are put at the corners of the flight path. The left figure shows the positions of those tags in the daytime. The right figure shows we are testing the estimator using an ARDrone (marked by the yellow rectangle) in the hall at night.

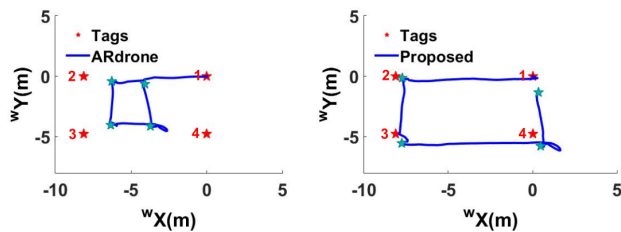


Fig. 10. Comparison of path estimation using an ARDrone. The left is the estimated path by integration of velocity from ARDrone itself; the right is the estimation by integration of velocity from our estimator. The four red stars represent the four corners of the flight path, the four green stars are the estimated positions when quadrotor is flying over each tag.

traveling distance. Our estimator however achieves better result with only  $1.37m$  drifting error and  $25.81m$  traveling distance.

## VII. CONCLUSIONS

This paper proposed a state estimator fusing the aerodynamic model of multi-rotor UAVs with measurements from optical flow, as well as other sensors that are commonly seen on multi-rotor UAVs. An extended Kalman filter is used to implement this estimator with state including both attitude and velocity. In addition, the drag coefficients are also included into state vector to account for rotor speed changes. Experimental results show that this estimator performs super robustness compared with existing methods and works well in low light conditions where vision-based methods usually fail. Furthermore, lower computational complexity than existing vision-inertial based systems allows the proposed estimator to be a low-cost, easily-implemented indoor positioning sensor.

## REFERENCES

- [1] Andrew J Davison, Ian D Reid, Nicholas D Molton, and Olivier Stasse. Monoslam: Real-time single camera slam. *IEEE transactions on pattern analysis and machine intelligence*, 29(6), 2007.
- [2] Georg Klein and David Murray. Parallel tracking and mapping for small ar workspaces. In *IEEE & ACM Proc. of Int'l Sym. on Mixed and Augmented Reality*, pages 225–234. IEEE, 2007.
- [3] Raul Mur-Artal, Jose Maria Martinez Montiel, and Juan D Tardos. Orb-slam: a versatile and accurate monocular slam system. *IEEE Trans. on Robotics*, 31(5):1147–1163, 2015.
- [4] Friedrich Fraundorfer and Davide Scaramuzza. Visual odometry: Part ii: Matching, robustness, optimization, and applications. *IEEE trans. Robotics and Automation Magazine*, 19(2):78–90, 2012.
- [5] David Nistér, Oleg Naroditsky, and James Bergen. Visual odometry. In *Proc. IEEE Conf. Computer Vision & Pattern Recognition*, volume 1, pages I–I. Ieee, 2004.

- [6] Simon Denman, Clinton Fookes, and Sridha Sridharan. Improved simultaneous computation of motion detection and optical flow for object tracking. In *Digital Image Computing: Techniques and Applications*, pages 175–182. IEEE, 2009.
- [7] Mandyam V Srinivasan. An image-interpolation technique for the computation of optic flow and egomotion. *Biological Cybernetics*, 71(5):401–415, 1994.
- [8] Dinuka Abeywardena, Shoudong Huang, Ben Barnes, Gamini Dissanayake, and Sarath Kodagoda. Fast, on-board, model-aided visual-inertial odometry system for quadrotor micro aerial vehicles. In *Proc. IEEE Int. Conf. Robotics and Automation*, pages 1530–1537. IEEE, 2016.
- [9] Dinuka Abeywardena, Zhan Wang, Sarath Kodagoda, and Gamini Dissanayake. Visual-inertial fusion for quadrotor micro air vehicles with improved scale observability. In *Proc. IEEE Int. Conf. Robotics and Automation*, pages 3148–3153. IEEE, 2013.
- [10] Guillaume Allibert, Dinuka Abeywardena, Moses Bangura, and Robert Mahony. Estimating body-fixed frame velocity and attitude from inertial measurements for a quadrotor vehicle. In *IEEE Conf. on Control Applications (CCA)*, pages 978–983. IEEE, 2014.
- [11] R Mahony, V Kumar, and P Corke. Multirotor aerial vehicles: Modeling, estimation, and control of quadrotor. *roboticsautomationmagazine*, 19, 20–32. *IEEE Trans. Automatic Control*, pages 1–1, 2012.
- [12] Huizhong Zhou, Danping Zou, Ling Pei, Rendong Ying, Peilin Liu, and Wenxian Yu. Structslam: Visual slam with building structure lines. *IEEE Transactions on Vehicular Technology*, 64(4):1364–1375, 2015.
- [13] David Nistér, Oleg Naroditsky, and James Bergen. Visual odometry for ground vehicle applications. *J. Field Robotics*, 23(1):3–20, 2006.
- [14] Bruce D. Lucas and Takeo Kanade. An iterative image registration technique with an application to stereo vision. In *International Joint Conference on Artificial Intelligence*, pages 674–679, 1981.
- [15] Dominik Honegger, Lorenz Meier, Petri Tanskanen, and Marc Pollefeys. An open source and open hardware embedded metric optical flow cmos camera for indoor and outdoor applications. In *Proc. IEEE Int. Conf. Robotics and Automation*, pages 1736–1741. IEEE, 2013.
- [16] Mingyang Li and Anastasios I Mourikis. High-precision, consistent ekf-based visual-inertial odometry. *Int. J. Robotics Research*, 32(6):690–711, 2013.
- [17] Omar Aboutalib, Bruce Awalt, Alex Fung, Bea Thai, Jeremy Leibs, Timothy J Klausutis, Ric Wehling, and Matthew James. All source adaptive fusion for aided navigation in non-gps environment. In *Defense and Security Symposium*, pages 657509–657509. International Society for Optics and Photonics, 2007.
- [18] Philippe Martin and Erwan Salaün. The true role of accelerometer feedback in quadrotor control. In *Proc. IEEE Int. Conf. Robotics and Automation*, pages 1623–1629. IEEE, 2010.
- [19] Robert C Leishman, John C Macdonald, Randal W Beard, and Timothy W McLain. Quadrotors and accelerometers: State estimation with an improved dynamic model. *IEEE Control Systems*, 34(1):28–41, 2014.
- [20] David J Hanley and Timothy W Bretl. An improved model-based observer for inertial navigation for quadrotors with low cost imus. In *AIAA Guidance, Navigation, and Control Conference*, page 0105, 2016.
- [21] Mark W Mueller, Michael Hamer, and Raffaello D’Andrea. Fusing ultra-wideband range measurements with accelerometers and rate gyroscopes for quadcopter state estimation. In *Proc. IEEE Int. Conf. Robotics and Automation*, pages 1730–1736. IEEE, 2015.
- [22] Guillaume Allibert, Robert Mahony, and Moses Bangura. Velocity aided attitude estimation for aerial robotic vehicles using latent rotation scaling. In *Proc. IEEE Int. Conf. Robotics and Automation*, pages 1538–1543. IEEE, 2016.
- [23] Todd Lupton and Salah Sukkarieh. Visual-inertial-aided navigation for high-dynamic motion in built environments without initial conditions. *IEEE Trans. on Robotics*, 28(1):61–76, 2012.
- [24] W. Johnson. Helicopter theory. 1980.
- [25] Thomas Brox, Andrés Bruhn, Nils Papenberg, and Joachim Weickert. High accuracy optical flow estimation based on a theory for warping. In *Euro. Conf. Computer Vision*, pages 25–36. Springer, 2004.
- [26] Lorenz Meier, Petri Tanskanen, Lionel Heng, Gim Hee Lee, Friedrich Fraundorfer, and Marc Pollefeys. Pixhawk: A micro aerial vehicle design for autonomous flight using onboard computer vision. *Autonomous Robots*, 33(1-2):21–39, 2012.